Direct Calculations of Stable and Unstable ZND Detonations by the Space-Time Conservation Element and Solution Element Method

Surg-Jue Park[1] Sheng-Tao Yu[2] Ming-Chia Lai[3]
Mechanical Engineering Department
Wayne State University
Detroit, Michigan

Sin-Chung Chang [4] Philip C.E. Jorgenson[5]
NASA Lewis Research Center
Cleveland, Ohio

ABSTRACT

In the present paper, we report numerical calculations of stable and unstable ZND detonation waves by the method of Space-Time Conservation Element and Solution Element. Due to the finite-rate chemistry employed in the ZND model, a source term exists in the species equation, which is solved in conjunction with the continuity, momentum, and energy equations. In the context of the space-time method, a treatment for the stiff source term based on a volumetric integration over a space-time region is developed. As a contrast to the modern upwind schemes, no modulated Riemann solver or splitting method is used, thus the logic of the present scheme is much simpler. Nevertheless, unstable detonation waves can be accurately captured by using only five mesh nodes per half reaction length. Numerical accuracy of the present method is assessed by detailed comparisons between the theoretical solutions and the numerical results for both stable and unstable ZND waves.

1. INTRODUCTION

1.1 Advanced Propulsion Concepts

Recent interests in advanced propulsion concepts have remarkably rekindled the research activities in detonation waves. Over the past decades, air-breathing Pulse Detonation Engines (PDEs) as well as rocket based PDEs have received significant attention. In the combustion chamber of a PDE, detonation waves propagate through a premixed fuel/air mixture and produce large chamber pressures for propulsion. Because of traveling detonations, constant-volume combustion, i.e., the detonation branch of the Rankine-Hugoniot curve, with high operational frequencies can be achieved. As a result, PDE could be a promising high-performance propulsion device.

Furthermore, in the development of air-breathing hypersonic propulsion vehicles, oblique detonation waves have been proposed to be used to enhance mixing in the supersonic combustion inside scramjet engines. In such engines, combustion takes place in the lee of the overdriven oblique detonation waves, which are usually attached to a wedge-like surface. Therefore, the detailed characteristics of overdriven detonation waves are of concern for the performance of such combustors.

1.2 ZND Detonations

Research of detonation waves was pioneered by Zeldovich, von Neumann, and Doering, i.e., the ZND model, in which a steadily propagating detonation wave consisting of an ordinary compressible flow shock followed by a finite-rate reaction zone is postulated. This remarkable insight of the flow physics provided the preliminary knowledge of detonations. Further experimental evidence has shown that detonation waves are often unstable with transverse wave structure, and the pressure level of the von

[1] Ph.D. Candidate, Email: spark@fluid.eng.wayne.edu
[2] Associate Professor, AIAA Member, Email: styu@eng.wayne.edu
[3] Professor, AIAA Member, Email: lai@eng.wayne.edu
[4] Senior Aerospace Engineer, Email: vvscc@noboo.lerc.nasa.gov
[5] Aerospace Engineer, Email: aejorgen@lerc.nasa.gov

Neumann spike is usually significantly higher than that predicted by the ZND model.

The capability of accurate calculations of stable and unstable detonation waves is imperative for the further development of the above-mentioned advanced propulsion concepts. In developing new numerical methods for detonations, the ZND model is an ideal proving ground for assessing the accuracy and efficiency of the method employed.

The numerical calculation of the ZND detonation model was pioneered by Fickett and Wood [1]. They solved the one-dimensional ZND model equations using the method of characteristics in conjunction with a shock fitting method. Longitudinal instability waves were simulated in detail.

Bourlioux et al. [2,3] developed an advanced numerical method, composed of a high-order upwind scheme, a front tracking method, and an adaptive refinement algorithm, for direct calculations of detonations. They presented detailed comparisons between the theoretical solution and their numerical solution. Similar calculations were conducted by Quirk [4] using various upwind schemes and Papalexandris [5] using an unsplit upwind method.

1.3 The Objectives of the Present Work

The objective of the present work is to extend the Space-Time CE/SE method, originally developed by Chang and coworkers [6,7] to calculate the stable and unstable detonation waves. In order to assess the numerical accuracy, we conducted detailed comparisons between the theoretical solution and the numerical results. In particular, we want *to identify the number of mesh nodes required for an accurate resolution of the reaction zone* following the shock front.

The rest of this paper is organized as follows. In Section 2, a brief account of the CE/SE method will be provided. The numerical treatment for the stiff source terms associated with the finite-rate chemistry will be discussed. In Section 3, the theoretical model of the ZND detonations is presented. In Section 4, the numerical solutions by the CE/SE method for steady and unsteady ZND waves will be reported. We then offer some concluding remarks.

2. THE SPACE-TIME CE/SE METHOD

The details of the Space-Time CE/SE method have been extensively illustrated in the cited references. Here, only a brief discussion of the essential steps of the CE/SE method will be provided. We shall first discuss the conventional finite-volume methods, in which because space and time are not treated equally, the choice of the space-time geometry has been restricted. As discovered by Godunov, the classical Riemann problem was encountered in balancing the space-time flux. Thus a Riemann solver became an integral part of the modern upwind schemes. In the present space-time CE/SE method, however, due to an equal footing treatment of space and time, the resultant formula is flexible to allow a better choice of space-time geometry to calculate flux conservation. In particular, a zigzagging strategy was developed such that the Riemann problem was avoided in balancing the space-time flux. Moreover, the spatial gradients of the flow variables are also treated as the unknowns and they march in time hand in hand with the flow variables themselves. As a result, no Riemann solver or reconstruction step is used as the building block. The logic of the present method is much simpler. In the following subsections, we shall illustrate the basic concept of the space-time integration in the CE/SE method as a contrast to the conventional methods. We then illustrate the essential steps of the present method in calculating the detonations.

2.1 Conventional Finite-Volume Methods

The conventional finite-volume methods for solving conservation laws were formulated according to flux balance over a *fixed spatial domain*. The conservation laws state that the rate of change of the total amount of a substance contained in a fixed spatial domain V is equal to the flux of that substance across the boundary of V, i.e., $S(V)$. Let the density of the substance be u and its spatial flux be $\boldsymbol{f}$, the convection equation can be written as

$$\frac{\partial u}{\partial t} + \frac{\partial \boldsymbol{f}}{\partial x} = \tau(u) \qquad (2.1)$$

where $\tau(u)$ is the source term in the convection equation. According to the Reynolds transport theorem, the integral form of the above equation can be expressed as:

$$\frac{\partial}{\partial t}\int_V u dV = -\int_{S(V)} \boldsymbol{f} \cdot d\vec{s} + \int_V \tau(u)\, dV \qquad (2.2)$$

The conventional finite-volume methods concentrated on calculating the surface flux, i.e., the first term on the right hand side. The time derivative term is usually treated by a finite difference method, e.g., the Runge-Kutta method. Or, integration can be performed for temporal evolution:

$$\int_V u dV \Big|_{t_1}^{t_2} = \int_{t_1}^{t} \left(-\int_{S(V)} \boldsymbol{f} \cdot d\vec{s} + \int_V \tau(u)\, dV \right) dt \qquad (2.3)$$

Due to the *fixed spatial domain*, the shape of the space-time Conservation Elements (CEs) in one spatial dimension for Eq. (2.3) must be rectangular. Refer to Fig. 2.1(a). The unknowns are usually placed at the center of the spatial mesh, i.e., on the boundary of the space-time CEs. The CEs must stack up exactly on the top of each other in the temporal direction, i.e., no staggering of these elements in time is allowed. For equations in two space dimensions, as depicted in Fig. 2.1(b), a conservation element is a uniform-cross-section cylinder in the space-time domain, and again no staggering in time is allowed.

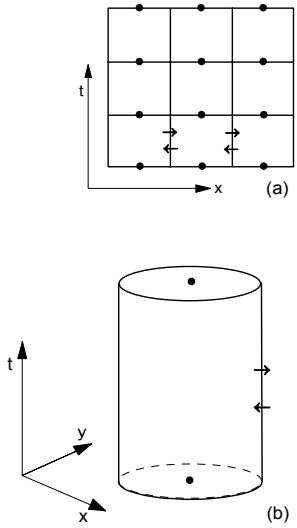

Fig. 2.1 Space-time integration for conventional finite-volume methods in one and two spatial dimensions.

This arrangement results in vertical interfaces extended in the direction of time evolution between adjacent space-time conservation elements. Across these interfaces, flow information travels in both directions. Therefore, an upwind bias method (or a Riemann solver) must be employed to calculate the interfacial fluxes.

2.2 The Space-Time Integration

Consider an initial-value problem involving the PDE,

$$\frac{\partial u}{\partial t} + a\frac{\partial u}{\partial x} = \tau(u) \qquad (2.4)$$

where a is a constant and $\tau(u)$ is a function of u. Let $x_1 = x$ and $x_2 = t$, be the coordinates of a two-dimensional Euclidean space E_2. Thus Eq. (2.4) becomes a divergence free condition,

$$\nabla \cdot \boldsymbol{h} = \tau(u) \qquad (2.5)$$

where the current density vector $\boldsymbol{h} = (au, u)$. By using Gauss' divergence theorem in the space-time E_2, it can be shown that Eq. (2.4) is the differential form of the integral conservation law:

$$\oint_{S(R)} \boldsymbol{h} \cdot d\vec{s} = \int_R \tau(u)\, dR \qquad (2.6)$$

Figure 2.2 is a schematic for Eq. (2.6).

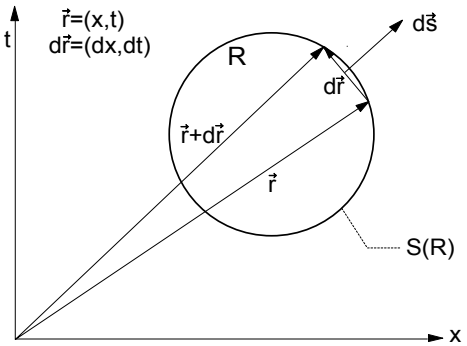

Fig. 2.2 A schematic of the space-time integral.

Here $S(R)$ is the boundary of an arbitrary space-time region R in E_2, $d\vec{s} = d\sigma\, \vec{n}$ with $d\sigma$ and $\vec{n}$, respectively, being the area and the outward unit normal of a surface element on $S(R)$, and dR is the volume of a space-time region inside $S(R)$. Note that $\boldsymbol{h} \cdot d\vec{s}$ is the space-time flux of $\boldsymbol{h}$ leaving the region R through the surface element $d\vec{s}$, and all mathematical operations can be carried out since E_2 was an ordinary two-dimensional Euclidean space. We remark that space and time are treated on an equal footing manner. Therefore, there is no restriction on the space-time geometry of the conservation elements over which the space-time flux is imposed.

Let Ω denote the set of all staggered space-time mesh nodes (j, n) in E_2 (dots in Fig. 2.3(a)) with n being a half or whole integer, and $(j - n)$ being a half integer. For each $(j, n) \in \Omega$, let the solution element SE(j, n) be the interior of the space-time region bounded by a dashed curve depicted in Fig. 2.3(b). It includes a horizontal line segment, a vertical line segment, and their immediate neighborhood. For the discussions given in this paper, the exact size of this neighborhood does not matter.

For any $(x, t) \in$ SE(j, n), let $u(x, t)$ and $\boldsymbol{h}(x, t)$, respectively, be approximated by $u^*(x, t; j, n)$ and $\boldsymbol{h}^*(x, t; j, n)$ which we shall define shortly.

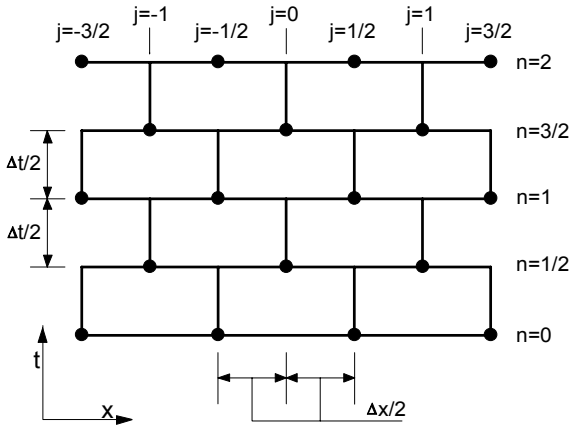

(a) The staggered space-time mesh

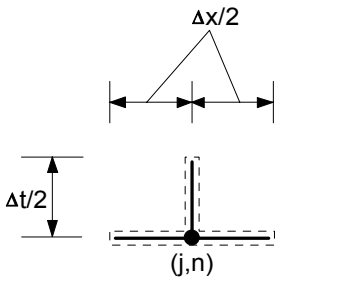

(b) SE(j,n)

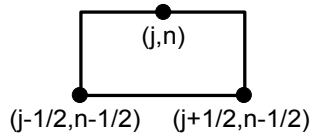

(c) CE(j,n)

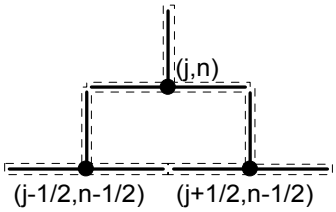

(d) The union of SE(j,n), SE(j-1/2,n-1/2) and SE(j+1/2,n-1/2)

Fig. 2.3 The space-time mesh of the CE/SE method.

Let

$$u^*(x, t; j, n) = u_j^n + (u_x)_j^n (x - x_j) + (u_t)_j^n (t - t^n) \tag{2.7}$$

where (i) u_j^n, $(u_x)_j^n$ and $(u_t)_j^n$ are constants in SE(j, n), and (ii) (x_j, t^n) are the coordinates of the mesh point (j, n). As will be explained later, we shall assume that

$$(u_t)_j^n = -a(u_x)_j^n \tag{2.8}$$

Combining Eqs. (2.7) and (2.8), one has

$$u^*(x, t; j, n) = u_j^n + (u_x)_j^n[(x - x_j) - a\,(t - t^n)], \quad (x, t) \in \mathrm{SE}(j, n) \tag{2.9}$$

As a result, there are two independent marching variables u_j^n and $(u_x)_j^n$ associated with each $(j, n) \in \Omega$. Furthermore, because $\boldsymbol{h} = (au, u)$, we define

$$\boldsymbol{h}^*(x, t; j, n) = (au^*(x, t; j, n), u^*(x, t; j, n)) \tag{2.10}$$

Let E_2 be divided into non-overlapping rectangular regions referred to as conservation elements (CEs). As depicted in Fig. 2.3(c), the CE with the midpoint of its top face being any mesh point $(j, n) \in \Omega$ is denoted by CE(j, n). The discrete approximation of Eq. (2.6) is

$$\oint_{S(CE(j,n))} \boldsymbol{h} \cdot d\vec{s} = \tau(u_j^n) \times \frac{\Delta x \Delta t}{2} \tag{2.11}$$

Here $\tau(u_j^n)$ is assumed to be the average value of $\tau(u)$ in CE(j, n). Because $(\Delta x \Delta t)/2$ is the volume of CE(j, n), Eq. (2.11) simply states that the total space-time flux of $\boldsymbol{h}^*$ leaving the boundary of any CE is equal to the source integral over the CE. Because the surface integration over any interface separating two neighboring CEs is evaluated using the information from a single SE, obviously the local conservation relation Eq. (2.11) leads to a global flux conservation relation, i.e., the total flux of $\boldsymbol{h}^*$ leaving the boundary of any space-time region that is the union of any combination of CEs is equal to the source integral over the same space-time region.

To justify Eq. (2.8), we shall assume that the value of u on a macro scale (that is the value of u obtained from an averaging process involving a few neighboring CEs) will not vary significantly as a result of redistribution of τ over each CE, in which τ is held constant. Based on this assumption, we take the liberty to redistribute the source term such that there is no source present within each SE. Thus with the aid of Eq. (2.7), Eq. (2.8) is the result of substituting $u = u^*(x, t; j, n)$ into Eq. (2.6).

Because the boundary of CE(j, n) is a subset of the union of SE(j, n), SE$(j\text{-}1/2, n\text{-}1/2)$ (refer to Fig. 2.3(d)), Eqs. (2.9-11) imply that

$$u_j^n - \frac{\Delta t}{2}\tau(u_j^n) = \frac{1}{2}[(1 - v)\,u_{j+1/2}^{n-1/2} - (1 - v^2)(u_x^+)_{j+1/2}^{n-1/2} + (1 + v)\,u_{j-1/2}^{n-1/2} + (1 - v^2)(u_x^+)_{j-1/2}^{n-1/2}] \tag{2.12}$$

Here, (i) $\nu \equiv (a\Delta t) / \Delta x$ is the Courant number and (ii) $(u_x^+)_j^n \equiv (\Delta x / 4)(u_x)_j^n$, $(j, n) \in \Omega$, is the normalized form of $(u_x)_j^n$. Given the values of the marching variables at the $(n - 1/2)$th time level, u_j^n is determined by solving Eq. (2.12) with the aid of Newton's iteration method. Note that, in the solver of the ZND wave, the initial estimated solution for Newton's iterations is calculated by assuming that the source term is zero. After u_j^n is known, $(u_x^+)_j^n$ is evaulated using a oscillation-suppressing procedure, which was described fully in [6,7]. Here, only a brief account si provided. Let $(j, n) \in \Omega$. With the aid of Eq. (2.8), we have

$$\begin{aligned} u'^n_{j\pm 1/2} &\equiv u^{n-1/2}_{j\pm 1/2} + \frac{\Delta t}{2}(u_t)^{n-1/2}_{j\pm 1/2} \\ &\equiv u^{n-1/2}_{j\pm 1/2} - 2\nu\,(u_x^+)^{n-1/2}_{j\pm 1/2} \end{aligned} \tag{2.13}$$

According to Eq. (2.13), $u'^n_{j\pm 1/2}$ can be interpreted as a first-order Taylor's approximation of u at $(j\pm 1/2, n)$. Let

$$\begin{aligned} (u^+_{x\pm})^n_j &\equiv \pm\,(u'^n_{j\pm 1/2} - u^n_j) \\ &= \pm\frac{\Delta x}{4}\,\frac{u'^n_{j\pm 1/2} - u^n_j}{\Delta x / 2} \end{aligned} \tag{2.14}$$

where $(u'^+_{x+})^n_j$ and $(u'^+_{x-})^n_j$, aside from a normalized factor $\Delta x/4$, are two numerical analogues of $\partial u/\partial x$ at (j, n) with one being evaluated from the right and the other evaluated from the left. Let the function W be defined by (i) $W(0, 0, \alpha) = 0$ and (ii)

$$W(x_-, x_+; \alpha) = \frac{|x_+|^\alpha x_- + |x_-|^\alpha x_+}{|x_+|^\alpha + |x_-|^\alpha} \tag{2.15}$$

Then $(u_x^+)_j^n$ is calculated using

$$(u_x^+)^n_j = W((u^+_{x+})^n_j, (u^+_{x-})^n_j, \alpha) \tag{2.16}$$

By using the procedures described in [6,7], the above scheme can be easily extended to become the solver of a nonlinear conservation equations with stiff source terms in either one-dimensional or multidimensional space. In addition to the present work, other CE/SE work related to the 1D and 2D problems with stiff source terms are presented in [8,9].

3. THEORETICAL MODEL

The classical ZND model of the one-dimensional detonation waves can be formulated by the Euler equations coupled with a species equation:

$$\frac{\partial \mathbf{Q}}{\partial t} + \frac{\partial \mathbf{E}}{\partial x} = \mathbf{S} \tag{3.1}$$

where **Q** is the unknown vector, **E** is the flux vector, and **S** is the source term:

$$\mathbf{Q} = \begin{pmatrix} \rho \\ \rho u \\ \rho E \\ \rho Y \end{pmatrix}, \quad \mathbf{E} = \begin{pmatrix} \rho u \\ \rho u^2 + p \\ (E+p)u \\ \rho u Y \end{pmatrix}, \quad \mathbf{S} = \begin{pmatrix} o \\ o \\ o \\ \dot{\omega} \end{pmatrix} \tag{3.2}$$

The four equations here are respectively the continuity, moment, energy, and species equations. In the equation set, ρ is density, u is velocity, p is pressure, Y is the mass fraction of the reactant, and $E = e + Yq + u^2/2$ is the total energy with e as the internal energy and q as the heat release. In species equation, a source term exists due to a one-step, irreversible chemical reaction, modeled by finite-rate kinetics. The source term can be expressed as

$$\dot{\omega} = -K\,exp(-E^+/RT)\,\rho Y \tag{3.3}$$

where K is the pre-exponential factor of the Arrhenius kinetics, E^+ is the activation energy, and R is the universal gas constant.

To proceed, the above equations are non-dimensionalized based on the density and the velocity of unperturbed reactants, i.e., ρ_o, u_o. The total energy, the internal energy, and the specific kinetic energy are non-dimensionalized by using E_o, e_o, and u_o, respectivelly. In order to keep the equation system consistent, we specify that $E_o = e_o = u_o^2 = RT_o$. In addition, the steady half-reaction zone length is chosen as the characteristic length scale l_0, and the time scale $\tau_o = l_o/u_o$, where u_o is the characteristic velocity of the flow field.

4. RESULTS AND DISCUSSIONS

Figure 4.1 is a schematic of detonation waves. A piston supported detonation is traveling from left to right and the flow field is composed of: (i) the quiescent state of the reactant before the shock, (ii) a von Neumann spike with finite rate reaction, and (iii) the equilibrium state between the piston and the spike. Two types of detonation calculations are of concern: (1) *the piston problems*, in which the detonation waves are initialized by a moving piston into the reactant, and (2) *the instability problems*, in which a steady state ZND analytical solution is used as the initial condition with

the chosen flow parameters such that the flow field is unstable. In both cases, detailed comparisons between the analytical solutions and numerical solutions are conducted to assess the numerical accuracy of the space-time CE/SE method.

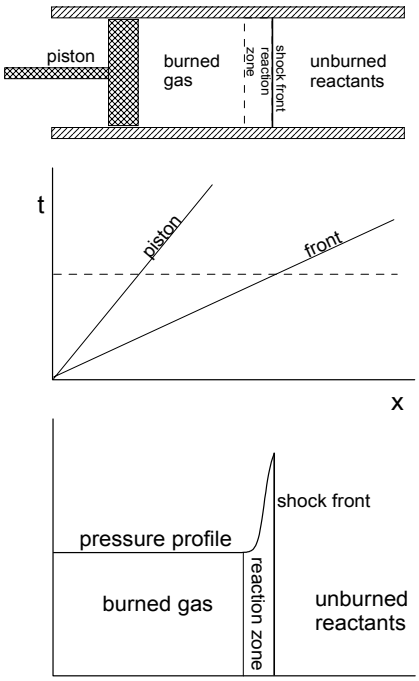

Fig. 4.1 A schematic of the ZND detonation wave.

4.1 The Piston Problems

The initial condition of the present calculation is a long tube filled with reactant with a piston on one end moving at a constant speed into the quiescent reactant. Here, we use the piston face as the origin of the coordinate system. According to this coordinate frame, reactant is charged into a closed-end tube at a constant speed. Thus, a shock wave is reflected on the closed end to ignite the reactant.

The parameters of the flow field in the present calculation are set as $q = 50$, $E^{+} = 50$, $\gamma = 1.2$, and the over drive coefficient equal to 1.8. According to the classical theory for detonation instability, a transient but stable detonation wave should be obtained with these parameters. In this calculation, 10 mesh nodes are used in the half reaction zone. Figure 4.2 shows the density distribution at $t = 100$. The numerical result shows a correct shock location as compared to the analytical solution

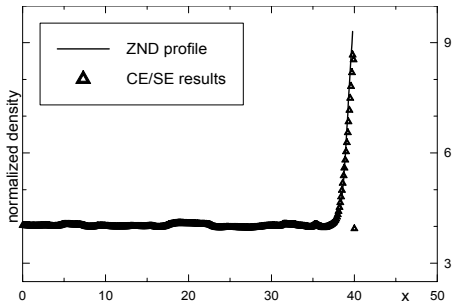

Fig. 4.2 Simulated shock propagation as compared to the analytical solution.

For the same calculation, Fig. 4.3 shows detailed comparisons of pressure, density, and reactant mass fraction profiles of the von Neumann spike. Excellent agreement is obtained between the analytical solution and the numerical solution by the CE/SE method.

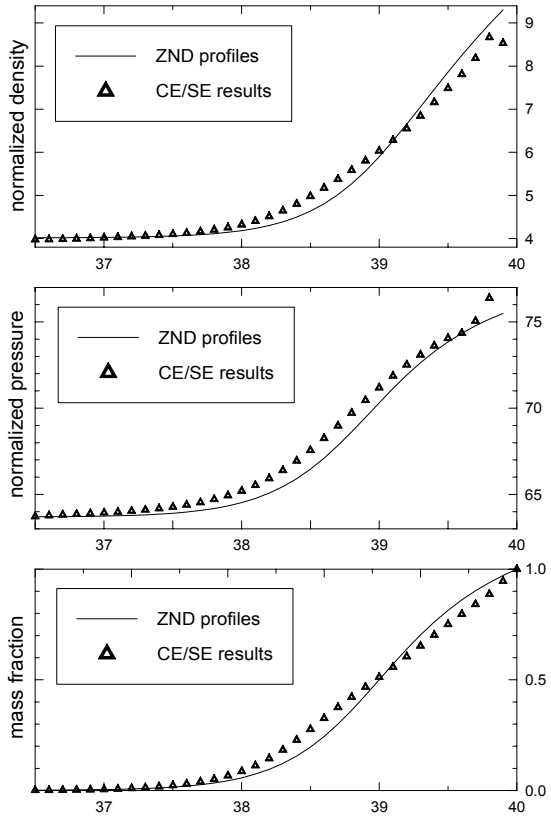

Fig. 4.3 Detailed of the von Neumann spike.

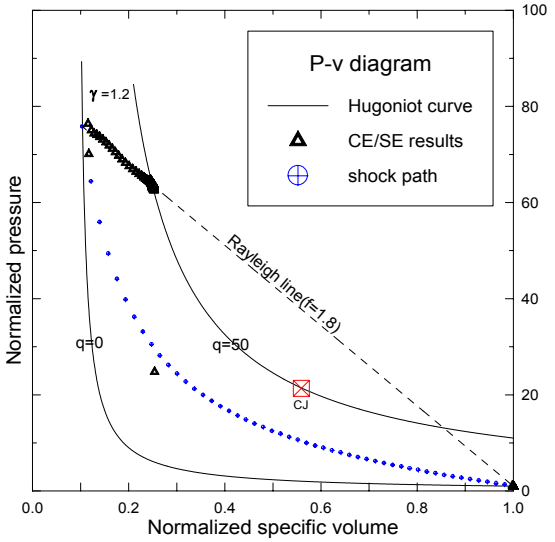

Fig. 4.4 The P-V diagram of a steady detonation.

To further investigate the accuracy of the CE/SE method, we shows the comparison between the numerical solution and the theoretical solution in the classical *P-V* diagram. The initial condition is $p = v = 1$ at the lower right corner of the plot. Note that the x axis and y axis are in different scales. Across the shock, the flow solution jumps to the intersection of the Hugoniot curve ($q=0$) and the Rayleigh line. In the figure, the theoretical shock path (denoted by small circular symbols) is calculated by the formula provided by White [10]. We remark that the intermediate flow solution inside the shock is controlled by the artificial damping added to the numerical scheme. Nevertheless, the numerical solution of p and v by the space-time CE/SE method are quite close to the theoretical shock path. In the reaction zone following the shock front, the numerical solution coincides with the Rayleigh line. In the equilibrium region, where the reaction is complete, the numerical solution converges to intersection of the Rayleigh line and the Hugoniot curve ($q=50$). Because of the overdriven factor ($f=1.8$), the p–v values in the reaction zone is much higher than the C-J point, which is denoted by a square symbol in Fig. 4.4. This figure demonstrates that the quality of the numerical result is comparable to that of the analytical solution.

If we lower the overdriven factor to 1.6, the detonation wave became unstable and a longitudinal wave bouncing between the piston and the shock front could be observed. In this calculation, only 5 mesh nodes are used in the each half-reaction zone. In Fig. 4.5, we show the temporal evolution of the pressure level at the shock front. The first pressure jump in the figure is caused by the start-up process of the pushing piston. After the first pressure jump, the flow field settles down and the instability waves gradually built up. After $t \geq 30$, a remarkable instability wave occurs. In about 50 time unit, there are about 8 pressure peaks. This numerical solution is in excellent agreement with the results reported by Fickett and Wood [1].

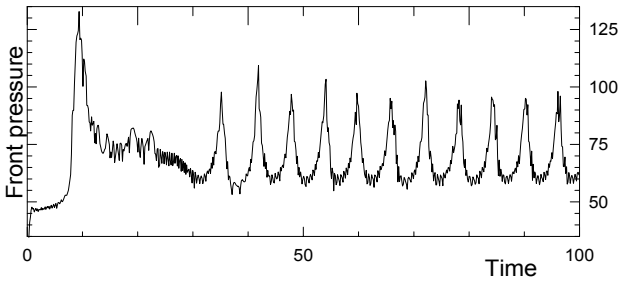

Fig. 4.5 The instability of the shock front of a piston problem.

4.2 The Instability Problems

In addition to the piston problems, we also conducted a mesh refinement study for the numerical resolution of the longitudinal instabilities of the detonation waves. To avoid the complexity of the start-up process of the pushing piston, the analytical solution of a stationary ZND detonation is used as the initial condition. In this case, the spatial coordinate is chosen such that the x coordinate of the shock front is zero. The parameters of the flow field in the present calculation are set as $q = 50$, $E^{+} = 50$, $\gamma = 1.2$, and the over drive coefficient equal to 1.6. Figures 4.6 (a), (b), and (c) show the temporal evolution of the pressure level of the shock front using 5, 10, and 20 grid nodes per half reaction zone, respectively.

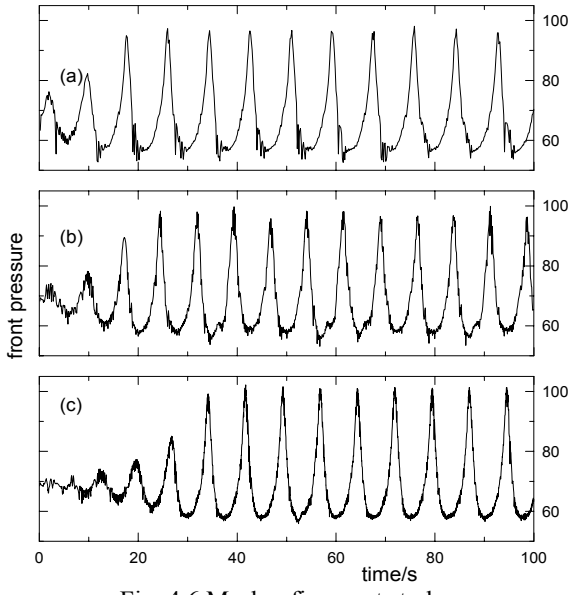

Fig. 4.6 Mesh refinement study.

The wave length of the oscillating pressure of the unstable shock front computed using the CE/SE method agrees very well with that obtained by Bourlioux [2]. Figure 4.7 shows the peak pressures obtained by various upwind schemes and the present method. In this figure, a relative mesh spacing of *w* corresponds to *10/w* points per half-reaction zone. Fickett and Wood established that for the above mentioned flow parameters the peak pressure is about 98.6. When fine meshes are used, all methods considered converge to that value.

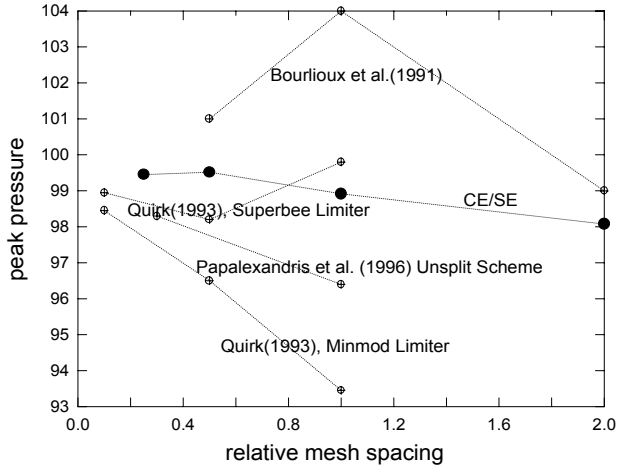

Fig. 4.7 Varaition of peak pressure predicted by different numerical methods with various mesh spacing.

5. CONCLUDING REMARKS

The space-time CE/SE method was conceived from a global CFD perspective and designed to avoid the limitations of the traditional methods. It was built from ground zero and with a foundation, which is solid in physics and yet mathematically simple enough that one can built from it a coherent, robust, and accurate CFD numerical framework.

In the present paper, the space-time CE/SE method has been extended and applied to solve the stable and unstable detonation waves. Detailed comparison between the analytical solution and the numerical solution has been conducted to assess the accuracy of the CE/SE method. Excellent numerical solution for unstable detonations can be obtained by using only 5 mesh nodes per half reaction zone.

ACKNOWLEDGEMENT

This work was performed under the support of NASA Lewis Research Center NCC3-580, and is part of an ongoing program at Wayne State University in applying the Space-Time CE/SE method to practical engineering problems.

REFERENCES

1. W. Fickett and W.W. Wood, "Flow Calculations for Pulsating One-Dimensional Detonations," *Physics of Fluids*, **9**(3) (1966) pp . 903-916.

2. A. Bourlioux, A. J. Majda, and V. Roytburd, "Theoretical and numerical structure for unstable one-dimensional detonations," *SIAM J. Appl. Math*., **51** (1991) pp. 303-343.

3. A. Bourlioux and A. J. Majda, "Theoretical and numerical structure of unstable detonations," *Phil. Trans. R. Soc. Lond. A*, **350** (1995) pp. 29-68.

4. J. J. Quirk "Godunov-Type Schemes Applied to Detonation Flows," ICASE Report No. 93-15, also NASA Contractor Report 191447, April 1993.

5. M. V. Papalexandris, "Unsplit numerical schemes for hyperbolic systems of conservation laws with source terms," Ph.D. Thesis, California Institute of Technology, 1997.

6. S.C. Chang, "The Method of Space-Time Conservation Element and Solution Element – A New Approach for Solving the Navier Stokes and Euler Equations," *J. Comput. Phys*., **119** (1995) pp. 295-324.

7. S.C. Chang, S.T. Yu, A. Himansu, X.Y. Wang, C.Y. Chow, and C.Y. Loh, "The Method of Space-Time Conservation Element and Solution Element – A New paradigm for Numerical Solution of Conservation Laws," to appear in *CFD Review 1997*, M.M. Hafez and K. Oshma eds., John Wiley and Sons, West Sussex, UK.

8. S.T. Yu and S.C. Chang, "Treatments of Stiff Source Terms in Conservation Laws by the Method of Space-Time Conservation Element and Solution Element," AIAA Paper 97-0435, 35th AIAA Aerospace Sciences Meeting, January 1997, Reno, NV.

9. S.T. Yu and S.C. Chang, "Applications of the Space-Time Conservation Element and Solution Element Method to Unsteady Chemically Reactive Flows," AIAA Paper 97-2007, in *A Collection of Technical papers*, 13th AIAA CFD Conference, June 1997, Snowmass, CO.

10. F.M. White "Viscous Fluid Flow," 1st ed., McGraw-Hill Book Co., New York, NY (1974) pp. 195- 202